Kalman Filter assisted Tracking of Microparticles in Hollow-Core Photonic Crystal Fibers for Sensor Applications

Max Koeppel[1,2*], Jasper Podschus[1], Nicolas Y. Joly[2,3,4,5], Philip St.J. Russell[3,4], Bernhard Schmauss[1,2,3]
[1]Institute of Microwaves and Photonics, Friedrich-Alexander University, Erlangen, Germany
[2]Graduate School in Advanced Optical Technologies, Erlangen, Germany
[3]Max Planck Institute for the Science of Light, Erlangen, Germany
[4]Department of Physics, Friedrich-Alexander University, Erlangen, Germany
[5]Interdisciplinary Center for Nanostructured Films, Erlangen, Germany
*max.koeppel@fau.de

Abstract: Accurate tracking of optically levitated microparticles inside hollow-core photonic crystal fibers is a key requirement for novel "flying particle sensors". We demonstrate a significantly improved tracking accuracy for accelerated particles by applying a Kalman filter.

1. Flying Particle Sensor

In the last decades, optical fiber sensors (OFSs) have found widespread application in a variety of fields covering monitoring of high-voltage transmission cables, structural health monitoring, fire detection and many others [1]. However, typical fiber sensors, which rely on discrete sensor elements or backscattering processes in the fiber, are either limited to predefined sensing locations or to relatively low spatial resolution—in the cm-range. A new type of OFS is based on optically levitated microparticles inside hollow-core photonic crystal fibers (HC-PCFs). Sensing of various quantities such as electric field and temperature by monitoring the particle response to external perturbations has been demonstrated [2]. Besides reconfigurability, these sensors can achieve very high spatial resolution while retaining the benefits inherent to fiber sensors such as immunity to electromagnetic interference and remote sensing. We have recently demonstrated a flying particle temperature sensor with a sub-mm spatial resolution, exploiting the temperature dependence of the viscosity of the air in HC-PCFs [3,4].

2. Doppler Optical Frequency Domain Reflectometry

To measure the position of a particle, we use Doppler optical frequency domain reflectometry (OFDR) as presented in [3,4], which is similar to frequency-modulated continuous-wave radar. A tunable laser source generates a linear optical frequency chirp, which is reflected by the trapped particle and interferes with a reference chirp at the photodetector (see Fig. 1(a)), generating a beat signal (see Fig. 1(b)). Particle movement and acceleration during the measurement cause phase distortion and broadening of the beat spectrum, which needs to be mitigated by auto-focus algorithms [3–5] in order to determine the beat frequencies $|f_{b,1}|$ and $|f_{b,2}|$ (see Fig. 1(b), (c)).

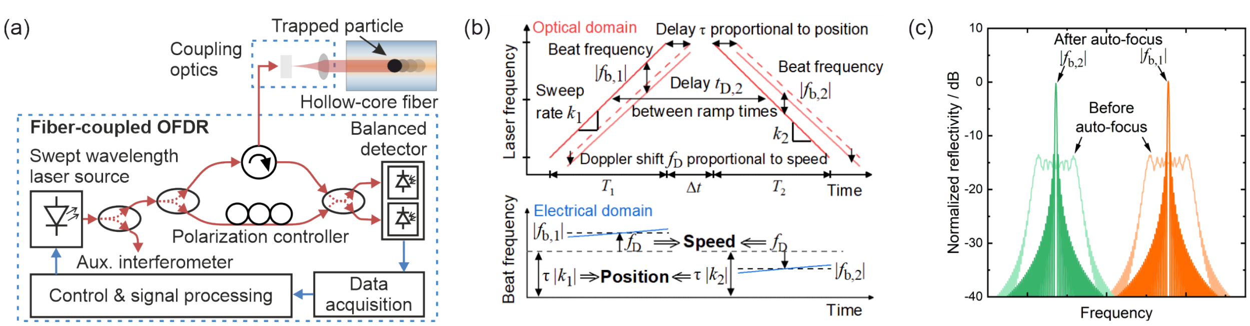

Fig. 1. (a) OFDR setup, (b) chirp signals and beat frequencies, (c) example beat spectra of an accelerated target (simulation).

Using the Doppler processing method presented in [3,4], the particle position z and speed v can be calculated from the beat frequencies $|f_{b,i}|$ (i = 1, 2). This method is suitable for uniform movement but introduces an error when the particle accelerates during the measurement. This effect becomes evident in the simulation shown in Fig. 2, where a steady target at z_0 = 1 m is accelerated at 75 mm/s² from 0.1 s to 0.3 s (100 simulation runs, sweep range: 1535 nm to 1545 nm, $T_1 = T_2$ = 5 ms, Δt = 3 ms delay between sweeps). In this case, the formulae derived for uniform movement lead to a localization error of approximately 233 µm and a speed error of around 488 µm/s during the acceleration.

3. Kalman Filter Implementation

However, as changes in the particle position and speed are interdependent, Kalman filtering can be applied to improve the accuracy of particle tracking during acceleration. We chose a discrete Wiener process acceleration model because the particle acceleration is caused by external perturbations that are not known a priori [6]. The state vector $\boldsymbol{x} = (z,\ v,\ a)^{\mathrm{T}}$ consists of the particle position z, speed v and acceleration a (the superscript T indicates the vector transpose) and the discrete system model is:

$$\boldsymbol{x}(t+1) = \boldsymbol{\Phi} \cdot \boldsymbol{x}(t) + \boldsymbol{\Gamma} \cdot w(t), \tag{1}$$

where $w(t)$ is a scalar zero-mean Gaussian noise process. The state transition matrix $\boldsymbol{\Phi}$, the noise gain vector $\boldsymbol{\Gamma}$ and the covariance matrix $\boldsymbol{Q}$ associated with the overall process noise $\boldsymbol{\Gamma}\cdot w(t)$ are [6]:

$$\boldsymbol{\Phi} = \begin{pmatrix} 1 & t_{\mathrm{M}} & t_{\mathrm{M}}^2/2 \\ 0 & 1 & t_{\mathrm{M}} \\ 0 & 0 & 1 \end{pmatrix}, \quad \boldsymbol{\Gamma} = \begin{pmatrix} t_{\mathrm{M}}^2/2 \\ t_{\mathrm{M}} \\ 1 \end{pmatrix}, \quad \boldsymbol{Q} = \frac{\sigma_w^2}{4} \begin{pmatrix} t_{\mathrm{M}}^4 & 2t_{\mathrm{M}}^3 & 2t_{\mathrm{M}}^2 \\ 2t_{\mathrm{M}}^3 & 4t_{\mathrm{M}}^2 & 4t_{\mathrm{M}} \\ 2t_{\mathrm{M}}^2 & 4t_{\mathrm{M}} & 4 \end{pmatrix}, \tag{2}$$

with $\sigma_w = 75$ mm/s², which is roughly the maximum acceleration increment over a whole measurement period t_{M} [6]. Instead of using the Doppler formulae presented in [3,4], we directly use the beat frequencies of an up and down chirp as system input in the measurement vector $\boldsymbol{z} = (f_{\mathrm{b},1}, f_{\mathrm{b},2})^{\mathrm{T}}$. Note that two independent measurements are necessary since the model is not observable for only one beat frequency input. The frequencies $f_{\mathrm{b},i}$ (after auto-focusing) for up ($i = 1$) and down ($i = 2$) chirps with start frequencies f_{0i}, sweep rates k_i, and sweep durations T_i, (see also Fig. 1(b)) are:

$$f_{\mathrm{b},i} \approx 1/c\left[2k_i z + \left(2f_{0i} + 2k_i t_{\mathrm{D},i} + 2T_i k_i\right) v + \left(f_{0i} T_i + k_i t_{\mathrm{D},i}^2 + 2T_i k_i t_{\mathrm{D},i} + 2f_{0i} t_{\mathrm{D},i} + 3k_i T_i^2/4\right) a\right], \tag{3}$$

where c is the speed of light (terms proportional to c^{-2} are negligible), and $t_{\mathrm{D},1} = 0$, $t_{\mathrm{D},2} = T_1/2 + T_2/2 + \Delta t$ takes the particle movement in between the ramps into account (see also Fig. 1(b)). Hence, the discrete measurement model

$$\boldsymbol{z}(t) = \boldsymbol{H} \cdot \boldsymbol{x}(t) + \boldsymbol{v}(t) \tag{4}$$

with the measurement noise vector $\boldsymbol{v}(t)$ uses the measurement sensitivity matrix $\boldsymbol{H}$:

$$\boldsymbol{H} = \frac{1}{c}\begin{pmatrix} h_{11} & h_{12} & h_{13} \\ h_{21} & h_{22} & h_{23} \end{pmatrix}, \tag{5}$$

where $h_{i1} = 2k_i$, $h_{i2} = 2f_{0i} + 2k_i t_{\mathrm{D},i} + 2T_i k_i$, $h_{i3} = f_{0i} T_i + k_i t_{\mathrm{D},i}^2 + 2T_i k_i t_{\mathrm{D},i} + 2f_{0i} t_{\mathrm{D},i} + 3k_i T_i^2/4$.

The covariance matrix $\boldsymbol{R} = \sigma_{\mathrm{f}}^2 \boldsymbol{I} = (125\ \mathrm{Hz})^2 \boldsymbol{I}$ (where $\boldsymbol{I}$ is the unit matrix) of the Gaussian measurement noise $\boldsymbol{v}(t)$ was adjusted to match the experimentally determined standard deviation $\sigma_z = 50$ µm of the OFDR position measurement for the given sweep parameters (1535 nm to 1545 nm in $T_1 = T_2 = 5$ ms, $\Delta t = 3$ ms delay between sweeps) and particle size (2 µm silica, see also [3,4]).

4. Results

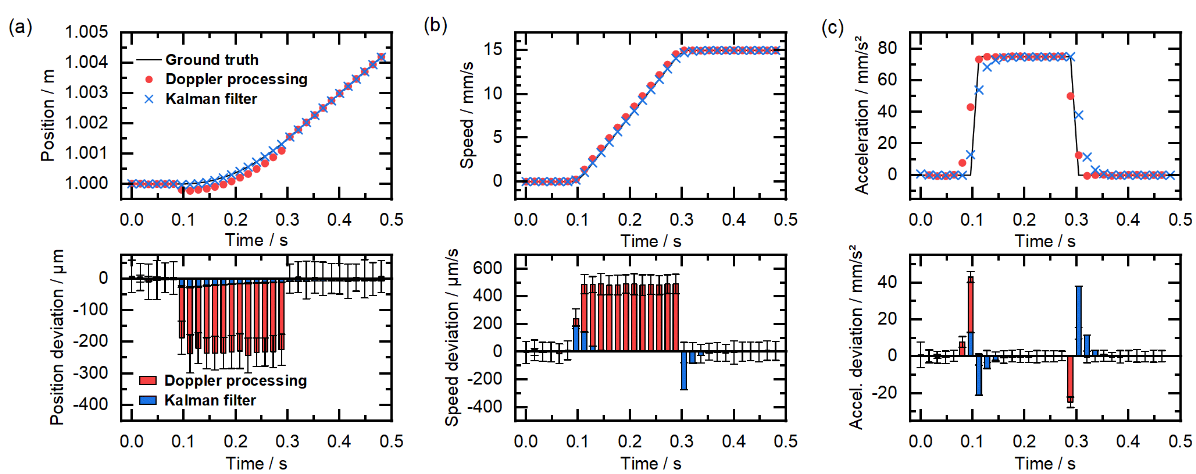

Fig. 2. Improved determination of target (a) position, (b) speed, and (c) acceleration by Kalman filtering for simulated data and deviation from the ideal values (the error bars indicate the standard deviation of 100 simulation runs).

We applied the Kalman filter to the above-mentioned simulation and achieved an improvement of the localization accuracy by more than a factor of 8 (233 µm to 27 µm deviation, see Fig. 2(a)) during acceleration. Likewise, the maximum speed deviation was reduced by more than one third from 488 µm/s to 273 µm/s (see Fig. 2(b)). The acceleration cannot be determined directly by Doppler processing, but can be calculated from the (inaccurate) speed differences of adjacent measurements. In contrast, the Kalman filter directly yields an acceleration value with slightly smaller maximum deviation and much smaller standard deviation (see Fig. 2(c)).

When the Kalman filter is applied to real measurement data, recorded while a particle was propelled with constant optical force along a heated fiber section (heater temperature: 200 °C, see [3,4] for details), the particle tracking is significantly improved during acceleration (see Fig. 3). While the Doppler processing method introduces an obvious position error (reduction of distance) as the particle approaches the heated fiber section (speed remains positive), the Kalman filtered position estimates agree with the expected trajectory (see Fig. 3(a)). The temperature gradient at the edges of the heated fiber section gives rise to thermal creep flow within the hollow core of the HC-PCF, causing rapid deceleration and a speed undershoot of the approaching particle (see Fig. 3(b)) [7]. The particle speed remains lower within the heated section due to changes in the viscosity of air [3,4,7]. Eventually, the particle is accelerated again by thermal creep flow when leaving the heated zone. This is in good agreement with [7] where Doppler velocimetry was used to track a particle. In the absence of acceleration, the Kalman filter output follows very closely the trajectory obtained by direct Doppler processing.

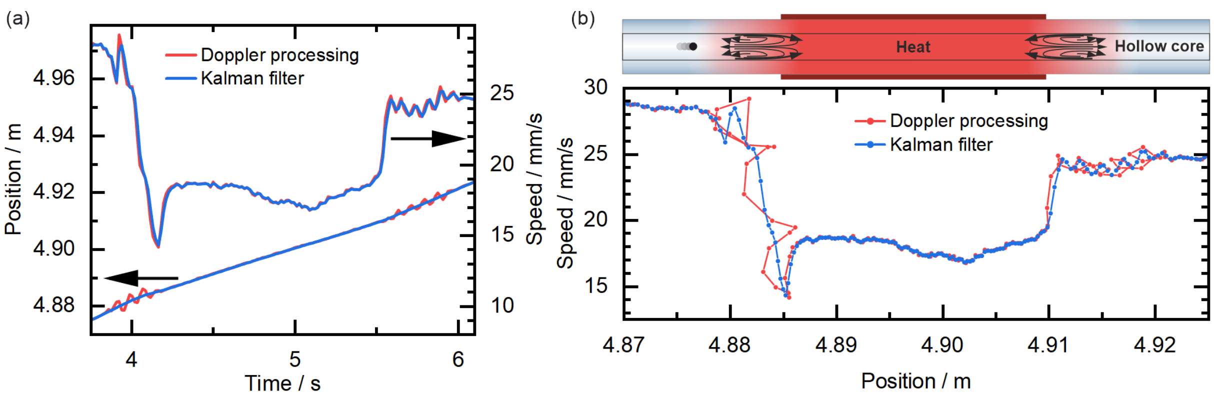

Fig. 3. Position and speed of particle flying through the heated fiber section (a) over time, (b) speed versus position.

5. Conclusions and Outlook

Kalman filtering can be used for more accurate OFDR tracking of the position, speed and acceleration of microparticles optically trapped inside a HC-PCF, especially during acceleration, as is the case in temperature sensing applications. In future work, the Kalman filter could be extended to more measurands, for example the detected particle reflectivity or trapping power variations, allowing the measurement uncertainty to be dynamically adjusted and thus further improving the tracking accuracy.

Acknowledgements

Parts of this research was funded by the Deutsche Forschungsgemeinschaft (DFG, German Research Foundation) under grant no. 418737652, the Max-Planck-Gesellschaft, and the Erlangen Graduate School of Advanced Optical Technologies (SAOT).

References

[1] A. H. Hartog, *An Introduction to Distributed Optical Fibre Sensors* (CRC Press, 2017).
[2] D. S. Bykov, O. A. Schmidt, T. G. Euser, and P. St.J. Russell, “Flying particle sensors in hollow-core photonic crystal fibre,” Nat. Photonics **9**, 461–465 (2015).
[3] M. Koeppel, A. Sharma, J. Podschus, S. Sundaramahalingam, N. Y. Joly, S. Xie, P. St.J. Russell, and B. Schmauss, “Doppler optical frequency domain reflectometry for remote fiber sensing,” Opt. Express **29**, 14615–14629 (2021).
[4] M. Koeppel, A. Sharma, J. Podschus, S. Sundaramahalingam, N. Y. Joly, S. Xie, P. St.J. Russell, and B. Schmauss, “Doppler optical frequency domain reflectometry for remote fiber sensing: erratum,” Opt. Express **29**, 24193 (2021).
[5] P. H. Eichel, D. C. Ghiglia, and C. V. Jakowatz, “Speckle processing method for synthetic-aperture-radar phase correction,” Opt. Lett. **14**, 1–3 (1989).
[6] Y. Bar-Shalom, X.-R. Li, and T. Kirubarajan, *Estimation with applications to tracking and navigation*, 1st ed. (Wiley-Interscience, 2001).
[7] O. A. Schmidt, M. K. Garbos, T. G. Euser, and P. St.J. Russell, “Reconfigurable optothermal microparticle trap in air-filled hollow-core photonic crystal fiber,” Phys. Rev. Lett. **109**, 24502 (2012).